ORIGINAL ARTICLE

Corrosion protection of carbon steel using a combination of Zr conversion coating and subsequent zinc-rich silicate coating with a flake ZnAl alloy

Nguyen Hoang [a],*, Truong Anh Khoa [a], Le Thi Nhung [a], Phan Minh Phuong [a], To Thi Xuan Hang [b], Nguyen Van Chi [c], Thanh-Danh Nguyen [d]

[a] *Nha Trang Institute of Technology Research & Application, Vietnam Academy of Science and Technology, Nha Trang, Viet Nam*
[b] *Institute for Tropical Technology, Vietnam Academy of Science and Technology, 18 Hoang Quoc Viet, Cau Giay, Hanoi, Viet Nam*
[c] *Coastal Branch, Vietnam - Russia Tropical Center, 30 Nguyen Thien Thuat, Nha Trang, Viet Nam*
[d] *Institute of Chemical Technology, Vietnam Academy of Science and Technology, TL29, Thanh Loc Ward, District 12, HoChiMinh City, Viet Nam*

Abstract   To improve the corrosion protection properties of zinc-rich silicate coatings on steel, zirconium pretreatment loaded with (3-aminopropyl)triethoxysilane (APTES) 0.025 % (v/v) and the partial replacement of spherical zinc by flake ZnAl alloy were investigated. DC polarization and electrochemical impedance spectroscopy (EIS) show that the zirconium pre-treated layer containing APTES improves the corrosion protection of the bare steel. Zinc-rich silicate coatings containing flake ZnAl with and without pretreatment were evaluated by EIS, salt spray test and pull-off test. Pretreatment with a zirconium conversion layer reduces corrosion products and adhesion loss (from 16.53% to 12.54%) while the performance of corrosion protection significantly increased from 2003 $\Omega.cm^2$ to 2640 $\Omega.cm^2$ in comparison with the non-pretreated samples. The results show that flake ZnAl pigment (5 wt%) significantly improves corrosion resistance and prolongs the duration of cathodic protection of zinc-rich silicate coatings.

* Corresponding author.
  E-mail address: nguyenhoangnt77@nitra.vast.vn (N. Hoang).
Peer review under responsibility of King Saud University.
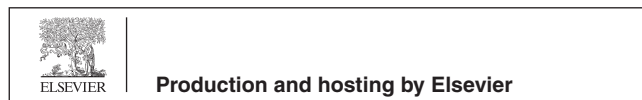
1. Introduction

Protection of bare steel from corrosion using coating methods is commonplace in industry. In many coating compounds, soluble inorganic silicates containing low volatility organic compounds are used as they have significant environmental advantages over organic silicate coatings, given the toxicity of organic solvents, such as benzene and ethanol (Del Amo et al., 2002; Deya et al., 2010; Ishimura et al., 2010).

Zinc-rich silicates are effective anti-corrosion coatings because of the more negative standard corrosion potential of zinc compared with steel (Abreu et al., 1996; Kalendova 2002; Giudice et al., 2004). Moreover, soluble zinc-rich inorganic silicate coatings have many beneficial features, as they are quick drying and have good rust resistance, weldability and mechanical performance, as well as low maintenance costs and a high level of safety (Selvaraj and Guruviah 1997; Meroufel and Touzain 2007; Shreepathi et al., 2010; Kakaei et al., 2013a,b). Thus, the efficiency of water-based inorganic silicate coatings is comparable to that of organic coatings (Parashar et al., 2003; Canosa et al., 2012).

The rate of delamination between the coating and the metal substrate is an important factor in evaluating the corrosion protection efficiency of a coating. The rate is highly dependent on adhesion between materials. Thus, pretreatment of the metal surface before coating is a key step, improving adhesion and thereby increasing corrosion resistance (Bajat et al., 2008; Saarimaa et al., 2021). Among many available methods, zirconium-based conversion coatings are a good choice for replacing conventional coatings as they can attain acceptable performance in typical operating conditions and temperatures (Fedrizzi et al., 2001; Verdier et al., 2005). It has been shown that a film on the metal surface formed in hexafluorozirconic acid (H_2ZrF_6) solution contains mainly ZrO_2 (Zhai et al., 2007; Ramanathan and Balasubramanian, 2016; Fockaert et al., 2017), which improves corrosion protection and adhesion and extends the duration of cathodic protection compared to samples without the Zr conversion coating (Golru et al., 2015; Sababi et al., 2017). With coatings of multiple layers of the nitrate salt of Zr and silane, double protection is formed, improving corrosion resistance by way of a uniform morphological surface and significantly reduced microcracks (Trabelsi et al., 2007; Abdelsalam et al., 2022).

Corrosion protection by zinc-rich coatings is the result of their cathodic and barrier protection properties. The cathodic protection mechanism is based on the separation of electrical contacts between the zinc particles and the metals within the coating (Barranco et al., 2004; Szociński and Darowicki 2016). Oxidation of zinc particles in a corrosive environment leads to a significant decrease in the zinc content of the coating, which is responsible for impaired electrical contact in these coatings (Marchebois et al., 2004; Ahadi and Attar, 2007). However, aluminium pigment can be mixed with a zinc-rich coating to reduce the oxidation of zinc particles (Feliu and Morcillo, 2001; Feliu Jr and Barranco, 2003). The aluminium powder in zinc silicate coating not only accelerates the cathodic protection effect but also reacts with the alkali metal silicate to produce insoluble silicate and form a thick protective film (Xu and He, 2019; Rajan et al., 2020). The barrier protection mechanism of zinc-rich coatings is based on the corrosion product formed from oxidation filling the fine pores in the coating, preventing penetration of the electrolyte solution into the coating and contact with the interface between the coating and the metal. However, the barrier mechanism is highly dependent on the zinc particle content and the morphology of the pigment particles (Kalendová, 2003).

Several recent reports have shown that Al pigments are effective co-protection agents in zinc-rich coatings, enhancing anticorrosion performance. For example, Zhang et al. (Zhang et al., 2012) investigated corrosion protection with Zn(Al) flake coatings and found that the flake ZnAl pigment significantly improves the protective ability of the zinc-rich coating. Arman et al. (Arman et al., 2013) showed that partial replacement of zinc dust particles by barrier micaceous iron oxide and Al particles enhances the anti-corrosion properties of the zinc-rich coating without reducing the sacrificial properties. Another report (Jalili et al., 2015) showed that replacing 2 wt% of zinc dust with aluminium nanoparticles in a standard zinc-rich epoxy coating improves its galvanic action and corrosion protection properties. Xu et al. (Xu and He, 2019) found that the properties of coatings, including adhesion strength, impact toughness, and alkali resistance, increase significantly when the waterborne zinc oxide-potassium silicate coating is modified by adding aluminium powder. Although the pretreatment of steel with a zirconium conversion layer has been shown to provide

good corrosion protection (Hosseini et al., 2014; Ramanathan and Balasubramanian, 2016; Sababi et al., 2017), to the best of our knowledge, the effect of both zirconium conversion layer and a flake ZnAl pigment on the corrosion behaviour of an inorganic silicate coating has not been studied. This work explores the influence of the partial replacement of spherical zinc particles with flake ZnAl alloy on the adhesion and anti-corrosion properties of water-based zinc-rich silicate coatings pretreated with the Zr conversion film.

2. Experimental

2.1. Material and sample preparation

The carbon steel sample used was CR1 steel complying with TCVN 7858:2018 (ISO 3574:2012) in different compositions e.g. 0.15 % C, 0.42% Mn, 0.05% P, 0.035 %S and 0.04% Al (wt%), and balanced Fe. Bare steel samples (10 cm × 15 cm × 0.1 cm) were sanded with 600, 800, 1000 and 1200 sandpaper, then degreased in methanol solution under ultrasonic conditions. The samples were later rinsed with deionized water and dried at room temperature.

The steel samples were pretreated with a Zr conversion coating before the application of a zinc-rich coating. A Zr-based conversion coating solution of hexafluorozirconic acid at a concentration of Zr^{4+} (50 ppm) was prepared by dissolving ZrF_4 in HF with distilled water. Then, (3-aminopropyl) triethoxysilane (APTES; Silquest A-1100, Momentive Performance Materials Inc., USA) was added to the H_2ZrF_6 conversion solution at a silane concentration of 0.025 % (v/v). Based on previous reports (Montemor et al., 2000; Hosseini et al., 2014; Asemani et al., 2016), the pH of the solution was adjusted to 4 by adding NaOH solution (0.1%), with magnetic stirring at 300 rpm to attain a homogeneous solution. The cleaned bare steel samples were immersed in a Zr conversion coating solution for 4 min, then the pretreated samples were washed with distilled water and dried in hot air at 70 °C (Trabelsi et al., 2005). To prepare the zinc-rich inorganic silicate coating, a nano-silica solution with particle size 9–10 nm (Vietnam Investment Casting Ltd. Co.) was added to potassium silicate solution (Xingtai Ocean Chemical Company, China) to form a binder with a molar ratio of SiO_2: K_2O (5:1).

The additives used included Silquest A187 (dispersing agent, Momentive Performance Materials Inc., USA) and tributine phosphate (antifoaming agent, Xilong Scientific Co., China). Different types of pigment, including spherical zinc with a mean particle size of 5–7 μm (Jotun Paint Company, Vietnam) and a mixture of spherical zinc and flake ZnAl alloy of 5–7 μm (ratio of Zn and Al is 80:20, Hunan Jinhao New Material Technology Co.) were used in the formulation of the zinc-rich coatings.

The mixtures were mechanically mixed for 20 min (1000 rpm). The steel surface with or without pretreatment with the Zr conversion coating was further coated with a zinc-rich silicate coating according to different coating formulations using a spray coating method. The zinc-rich coating was dried at room temperature in air. A coating thickness of 100 ± 10 μm was measured after 7 days of drying at room temperature. The surface morphology of spherical Zn and flake ZnAl alloy is shown in Figure S1.

Four different zinc-rich coatings were prepared using spherical Zn without pretreatment (M1, M2 and M3) and with pre-

treatment using a zirconium conversion coating (M4) at an optimal pigment mixture selected from samples M2 or M3. The composition and content of different pigments in the coatings are presented in Table 1.

2.2. Method

2.2.1. Electrochemical measurements

Electrochemical studies on bare and coated specimens were conducted using an Autolab PGSTAT 204N device. A three-electrode cell system was used for all experiments. The system was assembled with platinum as an auxiliary electrode, the test specimen as a working electrode, and an Ag/AgCl electrode as a reference electrode.

DC polarization was employed to investigate the corrosion current density (i_{corr}) and corrosion potential (E_{corr}) of the coated samples. The voltage was scanned at ± 150 mV with respect to open circuit potential (OCP) with a scan rate of 0.01 V/s.

The corrosion current density was obtained using the Tafel extrapolation technique at ± 50 mV around the OCP. EIS measurement was carried out on an area of 3.46 cm^2 for both Zr-based conversion and silicate coating samples, in NaCl 3.5% (w/w) solution in the frequency range of 100 kHz–0.01 Hz. The amplitude of the applied alternating potential was 10 mV peak to zero on OCP. For each sample, the test was carried out at least three times to ensure repeatability of the measurement. The acquired data were curve-fitted and analyzed using Nova 2.0 software.

2.2.2. Pull-off test

A pull-off adhesion test was performed with a Defelsko Positest AT (ASTM-D4541) for the measurement of adhesion strength of the silicate-based zinc-rich coatings of the samples with and without conversion zirconium coatings.

Dollies of 20 mm diameter were fixed onto the coated samples using two-part Araldite 2015 adhesive (Huntsman Advanced Materials, Germany). The samples were then kept at ambient temperature for 24 h to ensure that the glue was fully cured. Finally, a slot was made around the dollies and they were pulled at a speed of 10 mm/min normal to the coating surface until the silicate coating was detached from the steel substrate. All tests were carried out at least three times to ensure measurement repeatability

2.2.3. Salt spray test

A salt spray test was carried out in a salt spray cabin Q-FOG CCT600 according to JIS 8502: 1999. The rest of the coating surface was masked by a waterproof mixture of beeswax-colophony (3:1). The test was carried out at least three times to ensure the measurement repeatability.

Morphology and composition analysis of the Zr conversion layer was performed using field emission scanning electron microscope (FESEM) and energy-dispersive X-ray spectroscopy (EDS; Model Jeol 6490 JED 2300).

3. Results and discussion

The pretreatment of steel with a zirconium conversion layer is particularly important in enhancing the anti-corrosion performance of coatings. This study investigated the effect of this layer on the anti-corrosion properties and adhesion of water-based zinc silicate coatings. The flake ZnAl pigment was used to partially replace spherical pigments and reduce the oxidation of zinc particles in the inorganic coatings and provide insights into the degradation of zinc particles. The anti-corrosion behaviour and adhesion strength of the inorganic coatings with different pigments were investigated by electrochemical impedance spectroscopy (EIS) and salt spray testing. SEM images were used to evaluate the morphology of the coatings before and after the salt spray test. Finally, the effectiveness of the silicate coating pretreated with the Zr conversion film was evaluated by adhesion before and after the salt spray test.

3.1. The Zr-based conversion coating properties

The electrochemical properties of the Zr-based conversion coating before the coating process were investigated by EIS and DC polarization methods. The polarization curve was measured for the sample immersed in a NaCl solution (3.5%, w/w) to evaluate the corrosion resistance of the Zr conversion coating on the steel substrate. The polarization parameters extrapolated from the Tafel plots, including corrosion current density (i_{corr}) and corrosion potential (E_{corr}), are described in Table 2. Polarization resistance (R_p) is calculated according to the Stern–Geary equation (Golabadi et al., 2021):

$$R_p = \frac{\beta_a \beta_c}{2.303(\beta_a + \beta_c)i_{corr}} \tag{1}$$

As can be seen in Fig. 1 and Table S1, the steel substrate pretreated with Zr showed conversion coating (–637 mV) shifts to a more negative corrosion potential value compared to the bare steel sample (–599 mV). The anodic branch current density of the Zr conversion coating shifts to a lower value, contributing to the anodic inhibitory role of the zirconium

Table 1 Different composition and pigment content of silicate coatings.

Samples	Surface pretreatment	Spherical Zn content (%,w/w)	Flake ZnAl content (%, w/w)
M1	No	70	0
M2	No	50	5
M3	No	50	10
M4	Zr-based conversion	50	5

Table 2 Adhesive strength of zinc-rich silicate coatings with and without flake ZnAl pigments before and after immersion in NaCl solution (3.5 wt%) for 7 days.

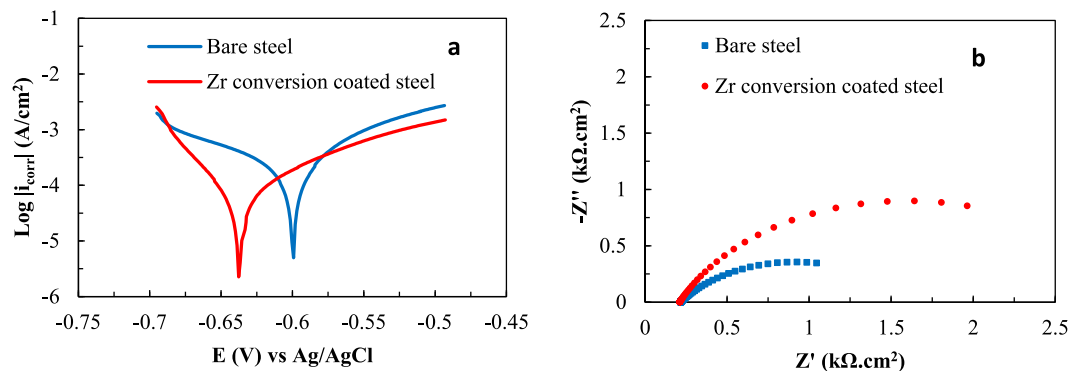| Samples	Adhesion (MPa)		Adhesion loss (%)
	Before immersion	After immersion	
M1	3.32 ± 0.15	2.68 ± 0.13	10.34
M2	3.71 ± 0.13	3.44 ± 0.08	4.67
M3	3.72 ± 0.14	3.28 ± 0.14	11.83

Fig. 1   DC polarization curves (a) and Nyquist diagrams (b) for bare steel sample and steel sample with Zr-based conversion coating.
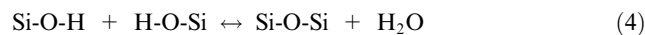
conversion coating and thereby preventing the metal dissolution of the bare steel (Golabadi et al., 2021). The pretreated steel sample has a much lower corrosion current density, indicating that a protective layer is formed on the surface of the steel, effectively blocking the active sites and limiting the diffusion of electrolytes onto the steel surface (Askari et al., 2014). In addition, polarization resistance represents the corrosion resistance of a material surface in aggressive environments and is determined from the diameter of the semicircles (Mohammadloo et al., 2012) in the Nyquist plots (Figure S2b). These plots show a single semicircle, which is indicative of a double layer on the surface between the electrolyte and coating. In addition, the semicircular curve of the Zr conversion coating has a larger diameter, confirming that the steel sample pretreated with the Zr conversion coating has better anti-corrosion performance, with a higher R_p value. From the experimental data, it can be seen that the value of current density is smaller, the corrosion potential is more negative, and the polarization resistance of the zirconium conversion layer on the steel base is larger than previously published research results at pH 4 (Hosseini et al., 2014; Asemani et al., 2016). This may be due to the effect of a double film with the zirconium conversion layer and the APTES 0.025% (v/v) silane additive (Montemor et al., 2000). In the APTES molecule, the ethoxy functional group (-OC$_2$H$_5$) easily bonds to the metal, while the amino group (–NH$_2$) can bond to the coating surface. Thus, APTES acts as a bridge between the metal surface and the coating (Xanthos 2010). The previous study (Golabadi et al., 2021) found that with the double-layer structure of the zirconium oxide film on the steel surface on the inside and a dominant silane film on the outside, the zirconium conversion layer reduces the number of active sites on the substrate surface, thereby limiting electrochemical processes in the cathodic reaction and enhancing the corrosion protection properties of the zirconium conversion layer.

The surface morphology and elemental composition of the bare steel and the steel coated with a Zr conversion layer are shown in Fig. 2. The steel with a Zr conversion coating has a clear and uniform structure whereas the bare steel has fine cracks. It indicates that the steel surface is effectively covered with a corrosion protection layer by the Zr conversion coating (Asemani et al., 2016). The formation of the Zr conversion coating contributes to an electrochemical reaction on the steel surface in the zirconium conversion bath (Mohammadloo et al., 2012). On the surface, the metal is oxidized and dissolves

into the solution by an anodic reaction (Fe → Fe^{2+} + 2e), while the H$^+$ ions are reduced by a cathodic reaction (2H$^+$ + 2e → H$_2$↑). Consequently, H$_2$ZrF$_6$ is hydrolyzed to form a ZrO$_2$ film via chemical equation (2):

$$H_2ZrF_6 + Fe + H_2O \rightarrow ZrO_2 + Fe^{2+} + 4H^+ + 6F^- + H_2 \tag{2}$$
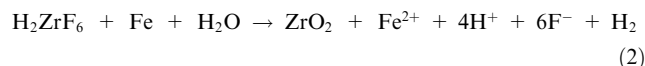
In the presence of APTES, the covalent bonds between the silane and the metal surface in the zirconium conversion solution are formed via chemical equations (3) and (4), and the siloxane network (Si-O-Si) can induce chemical stability of the conversion coating (Van Ooij et al., 2005; Zhan et al., 2017):

$$Metal\text{-}O\text{-}H + H\text{-}O\text{-}Si \leftrightarrow Metal\text{-}O\text{-}Si + H_2O \tag{3}$$

$$Si\text{-}O\text{-}H + H\text{-}O\text{-}Si \leftrightarrow Si\text{-}O\text{-}Si + H_2O \tag{4}$$

As can be seen in Fig. 2d, EDS analysis reveals the presence of the Zr element, confirming the successful coating of the Zr conversion layer. It is notable that most of the peaks are from elements of the bare steel substrate, indicating that the Zr conversion layer is very thin (Zhai et al., 2007). Thus, the results show that the formation of the conversion layer on the metal surface can be easily achieved in the presence of silane in the Zr solution with a low concentration (50 ppm) at pH 4.

3.2. Optimization of a zinc-rich silicate coating loading the flake ZnAl pigments

To achieve a simple experimental procedure for the optimization of the pretreatment, the partial replacement of spherical Zn with various levels of flake ZnAl alloy on the untreated bare steel was investigated. The optimum level for anti-corrosion performance was determined by evaluating coatings with and without pretreatment.

The surface morphology of the un-pretreated zinc-rich silicate coatings with different flake ZnAl content is shown in Fig. 3. The results reveal that sample M2 with 5 wt% flake ZnAl content has a smooth and uniform surface structure, while sample M1 without flake ZnAl alloy and M3 with a high content of flake ZnAl alloy have many cracks and a rough surface, which can reduce the anticorrosion effectiveness of the coatings.

The adhesive strength of a zinc-rich silicate coating with and without flake ZnAl pigment was investigated by a pull-
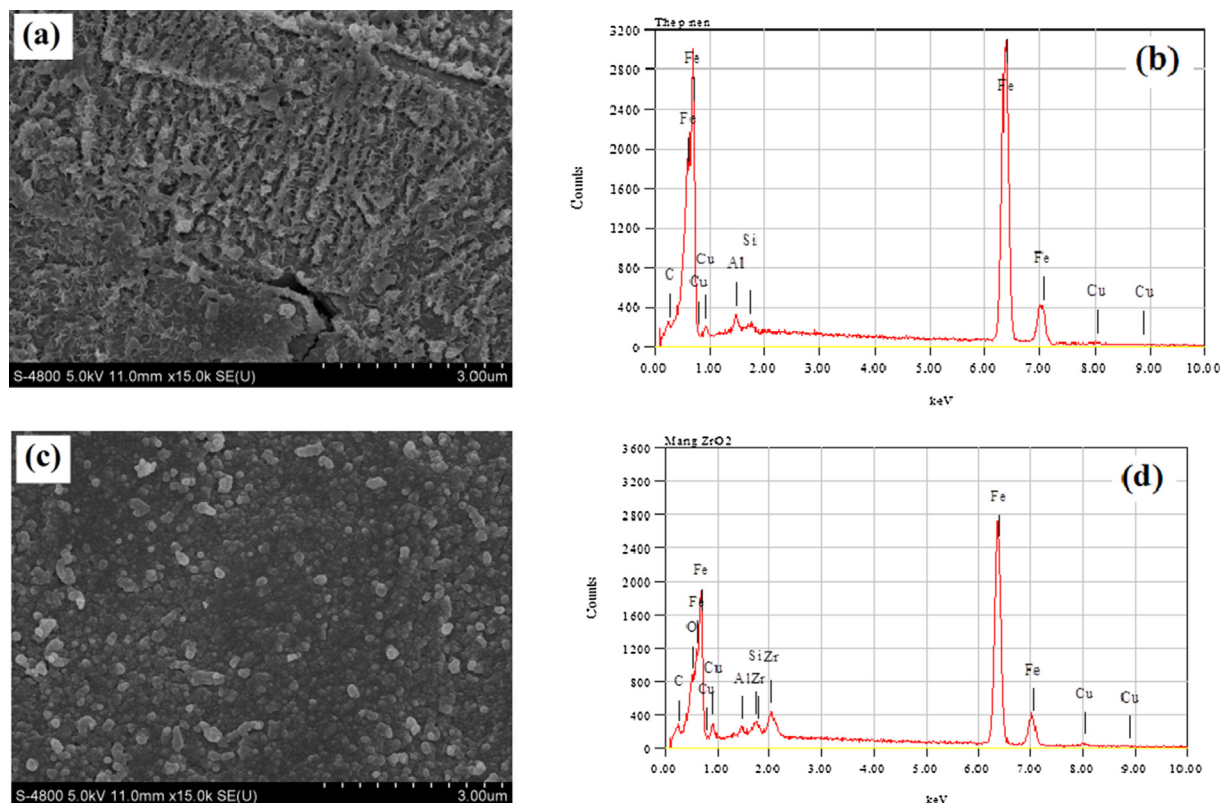
Fig. 2 SEM micrographs and EDS patterns of bare steel (a and b) and Zr conversion coated steel (c and d).
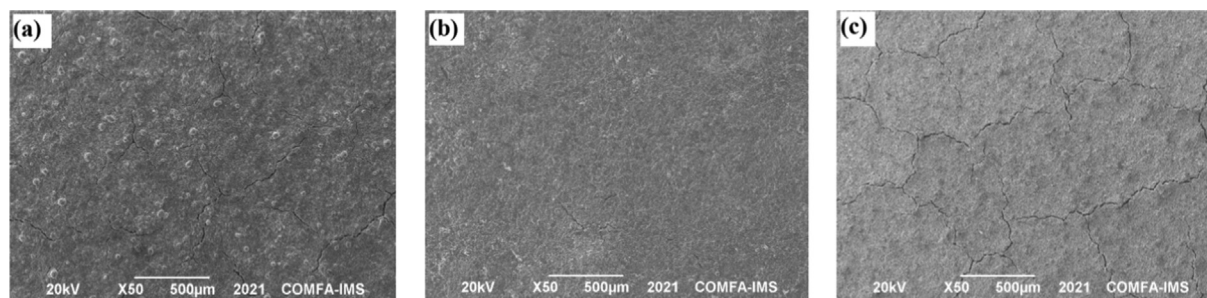

Fig. 3 The SEM micrographs of an un-pretreated zinc-rich silicate coating with flake ZnAl pigments: (a) sample M1 (70 wt% spherical Zn), (b) sample M2 (50 wt% spherical Zn + 5 wt% flake ZnAl alloy) and (c) sample M3 (50 wt% spherical Zn + 10 wt% flake ZnAl alloy).

of test in NaCl solution (3.5 wt%) for 7 days (Table 2). The decrease in adhesive strength is calculated by equation (5).

$$Adhesion\ loss(\%) = \frac{Adhesion\ before\ immersion - Adhesion\ after\ immersion}{Adhesion\ before\ immersion} \times 100$$

(5)

The least decrease in adhesive strength was observed for sample M2, confirming that the bonding force between the coating and the substrate is significantly enhanced by the flake ZnAl alloy. Meanwhile, sample M3 with higher flake ZnAl pigment content induces significant adhesion degradation, which contributes to electrolyte diffusion into the coating through surface defects and cracks causing the destruction of the adhesion bond, thereby reducing the anti-corrosion properties of the coating (Arman et al., 2013).

The anticorrosion performance of zinc-rich silicate coatings with flake ZnAl alloy at different concentrations was investigated using polarization curve analysis (Figure S2), as detailed in Table 3. The results show that the spherical Zn pigment induces substantial negative corrosion potential in all the samples compared to the standard potential of Ag/AgCl (-735 mV) (Kakaei et al., 2013a,b). This finding indicates that the active mechanism in zinc-rich coatings is mainly cathodic protection. It is notable that sample M2 with flake ZnAl alloy (5 wt%) has the most negative corrosion potential because the presence of both Zn and Al metals in the samples induces the corrosion potential of the coating (Abreu et al., 1996).

The results show that sample M1, with only 70 wt% spherical Zn, has the highest corrosion current density, indicating a strong oxidation rate of the spherical zinc particles. It was also

Table 3 Data from the DC polarization of a zinc-rich coating containing flake ZnAl pigment after immersion in NaCl solution (3.5 wt %) for 48 h.

Samples	E_{corr} (mV vs Ag/AgCl)	i_{corr} (μA/cm^2)	β_a (mV/dec)	- β_c (mV/dec)	R_p (Ω.cm^2)
M1	−1036.1	27.25	143.35	108.2	982.84
M2	−1067	8.80	84.80	72.86	1934.27
M3	−1034.4	23.26	134.6	117.93	1173.77

found that corrosion current density rapidly decreases in sample M2 with flake ZnAl alloy (5 wt%), revealing that the flake ZnAl pigment induces a significant reduction in the anodic reaction rate and contributes to a tighter arrangement of the ZnAl alloy with the spherical Zn pigment in the silicate coating, leading to the formation of a compact coating, which can be expected to improve the barrier protecting the metal surface from corrosive media. Sample M3, with a higher ZnAl flake content, has significantly higher corrosion current density, indicating a rapid increase in the anodic reactivity with flake ZnAl content. Excessive ZnAl content can reduce bond formation in the silicate coating, leading to cracks and holes in the coating that might increase the diffusion of the electrolyte and reduce the corrosion protection performance of the coating by the cathodic protection mechanism (Saeedikhani et al., 2019).

To evaluate the corrosion resistance of the coatings with different flake ZnAl contents, EIS spectrum analysis was employed to collect information on corrosion properties. The Nyquist and Bode plots of the silicate coatings for all the samples are shown in Fig. 4. The Nyquist plots show that the corrosion activity of all the samples after the immersion process is similar; this is because the coating formula includes mainly spherical Zn. The same semicircular curves represent electrolyte penetration into the defect sites on the coating surface (Zhang et al., 2010). The largest semicircle radius is observed for sample M2, with 5 wt% of flake ZnAl alloy, indicating improved corrosion protection by the silicate coating. Meanwhile, sample M3 has a lower semicircle radius, indicating a decrease in the effectiveness of corrosion protection due to an excessive amount of flake ZnAl alloy reducing the anticorrosion activity of the silicate coating. The low-frequency impedance modulus of sample M2 is the highest among the samples in the Bode plots. The barrier properties of the flake ZnAl pigment and its good reactivity in silicate solutions give sample M2 coatings better anti-corrosion properties than the other samples. A high phase angle for sample M2 observed in the Bode plots indicates its substantial coating resistance (Golabadi et al., 2021).

The experimental data of the EIS measurements fit the equivalent circuit model, which is $[R_s([R_c(R_{ct}C_{dl})]Q_c)]$ for all samples, where R_s, R_c, R_{ct}, C_{dl} and Q_c are corrosion solution resistance, coating resistance, charge transfer resistance, double-layer capacitance, and constant phase elements (CPEs), respectively. CPEs are used to replace ideal capacitors to account for the effects of roughness due to the random distribution of pigments and the heterogeneity of composition and structure (Kakaei et al., 2013a,b). The results also show a low R_{ct} value of sample M1, which is related to a high corrosion rate (Kakaei et al., 2013a,b). The R_{ct} value of sample M2 is much higher than that of the sample M3 (Table S2), indicating the lack of the silicate binder due to the large amount consumed when an excessive amount of flake ZnAl alloy is added to the solution (Xu and He, 2019). This phenomenon reduces the chemical reaction in the silicate solution and the number of zinc particles in the coating, leading to a decrease in the electrical contact between the zinc particles (Parashar et al., 2003). Moreover, the high R_{ct} value of sample M2 shows that flake ZnAl alloy can create a tight and parallel arrangement with the spherical Zn pigment. Also, flake ZnAl can form a bonding matrix in the silicate coating at suitable concentrations, reducing the diffusion of the electrolyte into the coating/substrate interface (Saeedikhani et al., 2019).
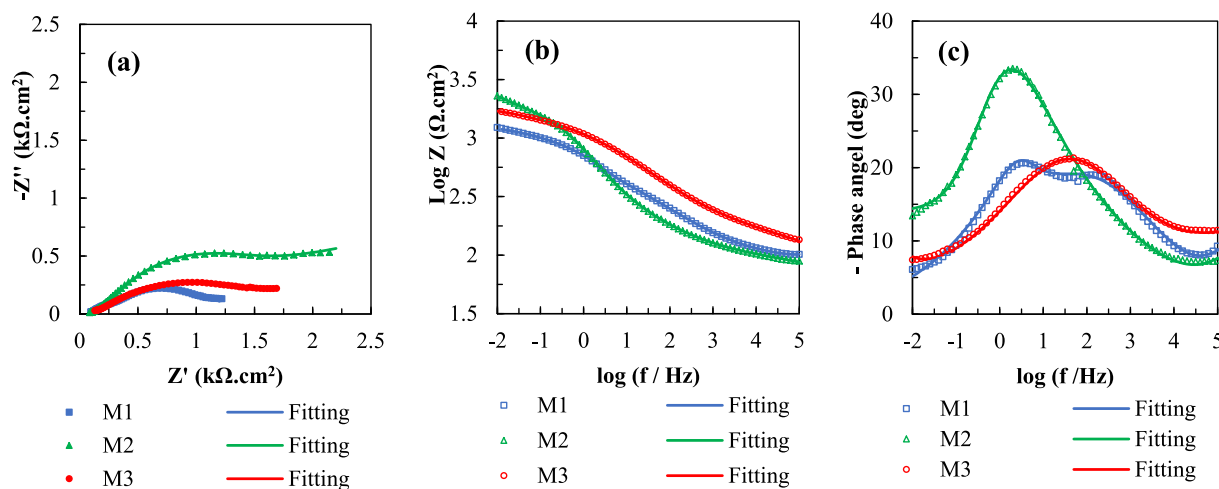
Fig. 4 Nyquist plots (a) and Bode plots (b and c) of zinc-rich silicate coatings for all samples after immersion in NaCl solution (3.5 wt%) for 2 days.

The analytical results show that a silicate coating with a mixture of flake ZnAl alloy (5 wt%) and spherical Zn particles can significantly enhance adhesion and corrosion protection properties, while an excessive amount of flake ZnAl in the coating reduces anticorrosion effectiveness. Therefore, the coating conditions of sample M2 were used to explore the effect on corrosion protection properties of pretreatment with a zirconium conversion layer.

3.3. Effect of flake ZnAl alloy on zirconium conversion pretreated zinc-rich coating

3.3.1. EIS measurements

The anticorrosion properties of samples M1, M2 and M4 coated with Zinc-rich silicate with and without zirconium conversion pretreatment were investigated using EIS measurements. The Nyquist and Bode plots of the samples measured in NaCl solution 3.5 wt% for 60 days are shown in Fig. 5. The semicircular diameters of all three samples increased with increasing immersion time. However, the impedance values of M2 and M4 slowly increased with a longer immersion time of 30 to 60 days at low frequency, indicating that the anticorrosion behaviour of spherical Zn and the flake ZnAl alloy in the coating is different. For sample M1, with only the spherical Zn coating, the corrosion products (zinc oxide) from the cathodic protection form and fill the holes in the coating, creating a barrier that increases impedance (Arman et al., 2013). When spherical Zn particles are partially replaced by flake ZnAl alloy in samples M2 and M4, the coating benefits not only from sacrificial anodic protection but also from a barrier protection mechanism due to the electrochemical activity of Al in the flake ZnAl alloy (Jalili et al., 2015). Sample M4 with zirconium pretreatment containing the flake ZnAl alloy after immersion for 60 days has the longest semicircular radius, and this relates to the good anti-corrosion properties of the coating (Cheng et al., 2019), confirming that the zirconium conversion coating enhances the anticorrosion properties of zinc-rich coatings containing flake ZnAl alloy.

The total resistance of the coating features a low-frequency impedance modulus (Hosseini et al., 2014). Thus, the corrosion behaviour of the Zn-rich silicate coatings can be observed via the plots of total impedance at the lowest frequency (10 mHz) versus immersion time, as shown in Fig. 6a. The results reveal that sample M1 containing only spherical Zn pigment has the lowest impedance after 2 days of soaking in a corrosive environment. The porous surface of sample M1 increases the diffusion of the electrolyte through the coating surface, leading to a rapid increase in the zinc particle oxidation rate. The ESI data show excellent electrical contact between the spherical zinc particles that results in the first pair of galvanic cells on the surface of zinc particles (Xia et al., 2021). In addition, the low-frequency impedance values of all the samples increase with immersion time. The highest impedance values are found with sample M4 at all immersion times, indicating that the Zr conversion coating has high corrosion protection efficiency compared to the un-pretreated samples because of its uniform structure and suitable roughness (Golabadi et al., 2021).

The plots of the phase angles at high frequency (100 kHz) versus immersion time obtained from the Bode plots indicate the protective performance of the coating (Fig. 6b) (Zand and Mahdavian, 2007). The data show that the phase angles of all the samples shift to more negative values with immersion time, contributing to an increase in the resistance of the coatings, obstructing the diffusion of the electrolyte into the coatings with immersion time (Jalili et al., 2015). The results also show that the pretreated sample M4 has the most negative phase angle value after 60 days of immersion in the corrosive solution, indicating that the zirconium conversion coating effectively reduces the diffusion of electrolytes towards the coating/substrate interface (Golabadi et al., 2021). This phenomenon is the result of the increased resistance of the coating-induced current through a capacitor shifted to a more negative phase angle, contributing to the current being $-90°$ out-of-phase with respect to voltage. Meanwhile, the phase angle of samples M1 and M2 shifts to positive values, indicating that the electrolyte can diffuse through the coating onto the coating/substrate interface.

3.3.2. Salt spray test

To evaluate the adhesive strength of the samples with and without pretreatment and their anticorrosion properties, a salt spray test was performed for 1000 h. The images of the coating surface after the salt spray test are shown in Fig. 7. Sample M1 coated only with spherical Zn particles has white rust on a scratch after 24 h. The protection coating with spherical Zn particles is well known to have cathodic and barrier protection properties (Barranco et al., 2004; Szociński and Darowicki, 2016). The data confirms that the sacrificial anodic protection of steel is destroyed after 24 h of salt spray. However, the white rust disappears on the surface after 360 h, which could be due to the porous corrosion product peeling from the pores and restoration of electrical contact between the zinc particles and zinc/bare metal. Thus, the coatings revert to a cathodic protection mechanism. This result confirms that the corrosion protection mechanism of the coating with only spherical Zn particles involves the restoration of the cathodic and barrier protection mechanisms in long-term corrosive environments (Grundmeier et al., 2000).

The salt spray test on sample M2 without the pretreatment layer shows white rust on the scratch after 360 h, confirming the anticorrosion behaviour of the coating with a cathodic protection mechanism (Kakaei et al., 2013a,b). Moreover, the absence of red rust after 1000 h demonstrates the effective protection of the substrate metal surface using flake ZnAl pigment in the coating as a result of its barrier properties.

It is notable that no corrosion products were observed for sample M4 pretreated with a zirconium conversion layer, with not even white rust after 1000 h. This result confirms the simultaneous cathodic and barrier corrosion protection effects of zinc-rich silicate coatings containing flake ZnAl alloy with the pretreatment. The result also indicates good maintainability of the electrical contact between zinc particles and zinc/base metal and improved protection that can prevent electrolyte diffusion onto the coating. This work indicates significant enhancement on the protection prolonging and efficiency in comparison with the previous reports (Zhang et al., 2012; Jalili et al., 2015; Xu and He, 2019). In addition, pretreatment with a zirconium conversion layer limits the electrochemical reactions occurring on the metal surface and controls the corrosion process under the coating (Golabadi et al., 2021).
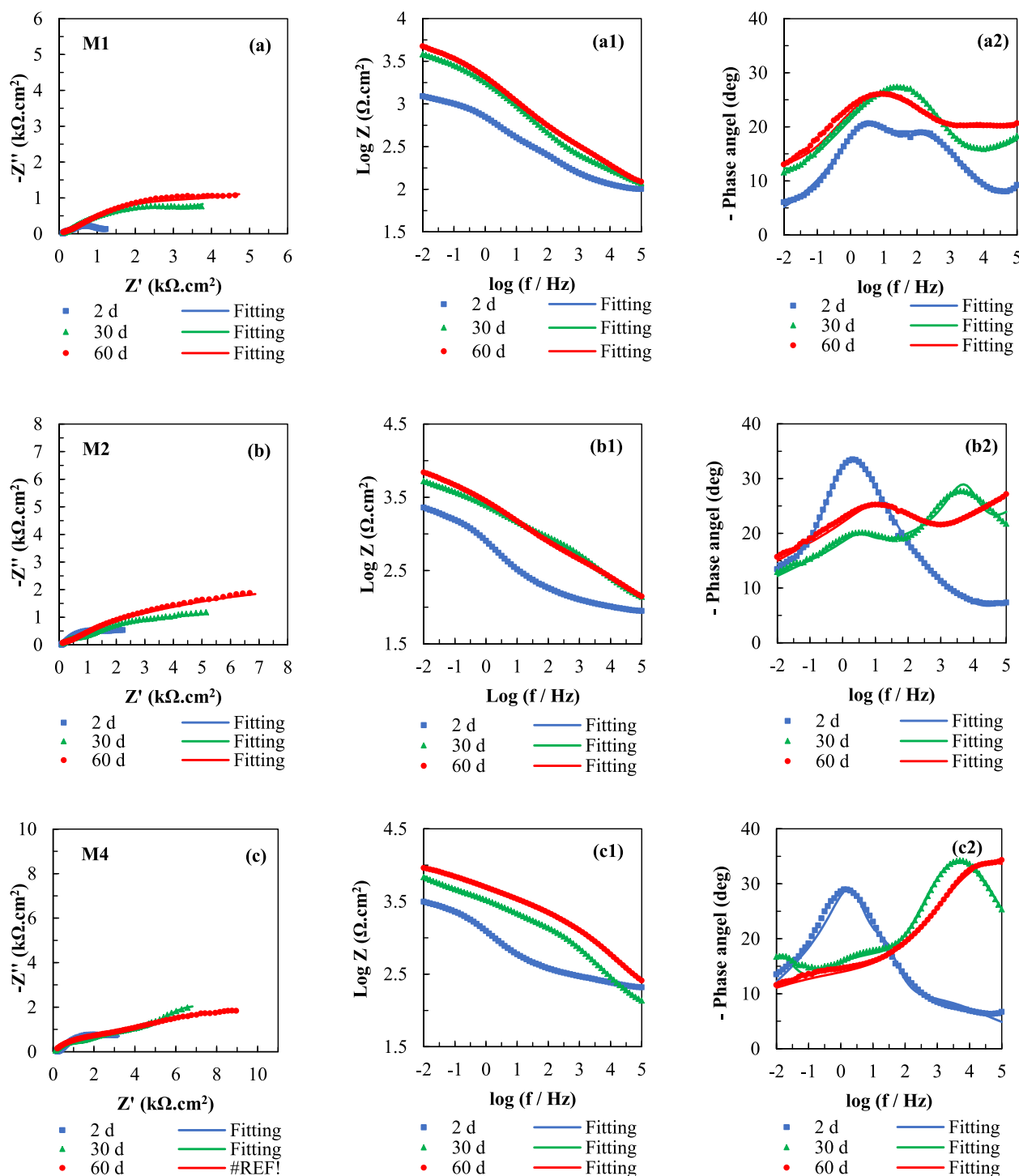
Fig. 5 Nyquist (a, b and c) and Bode (a1, a2, b1, b2, c1 and c2) plots of zinc-rich silicate coating with and without un-pretreated: un-pretreated sample M1 (70 wt% spherical Zn); unpretreated sample M2 (50 wt% spherical Zn and 5 wt% flake ZnAl) and Zr pretreated sample M4 (50 wt% spherical Zn and 5 wt% flake ZnAl) after immersion in NaCl solution (3.5 wt%) for 60 days.

3.3.3. Morphology of the silicate coating in the salt spray test

SEM images of the silicate coating surface before and after the salt spray test are shown in Fig. 8. Sample M1 shows a significant decrease in the number of spherical Zn particles after 1000 h (Fig. 8a1 and 8a2), confirming that corrosion products form on the coating surface and indicating that the spherical

Zn pigment is effectively consumed for cathodic corrosion protection over a long period up to 1000 h.

The SEM images of sample M2 without the pretreatment layer show that spherical and flake-like corrosion products appear on the surface and the number of zinc particles on the surface after the salt spray test is significantly lower in comparison with sample M4; this can cause effective preven-
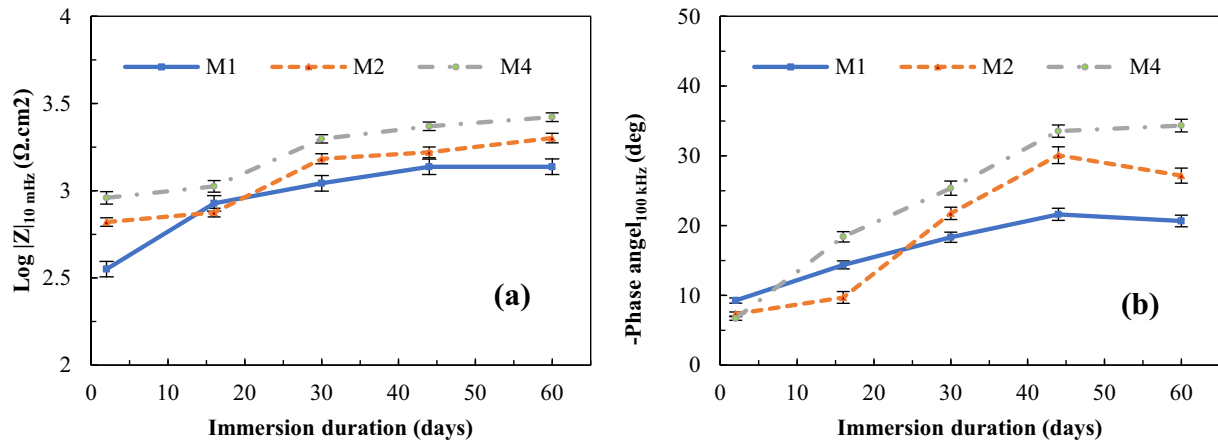
Fig. 6 The plots of total impedance at the lowest frequency (10 mHz) (a) and phase angle at the highest frequency (100 kHz) (b) against immersion time of the silicate coatings obtained from the Bode plots.
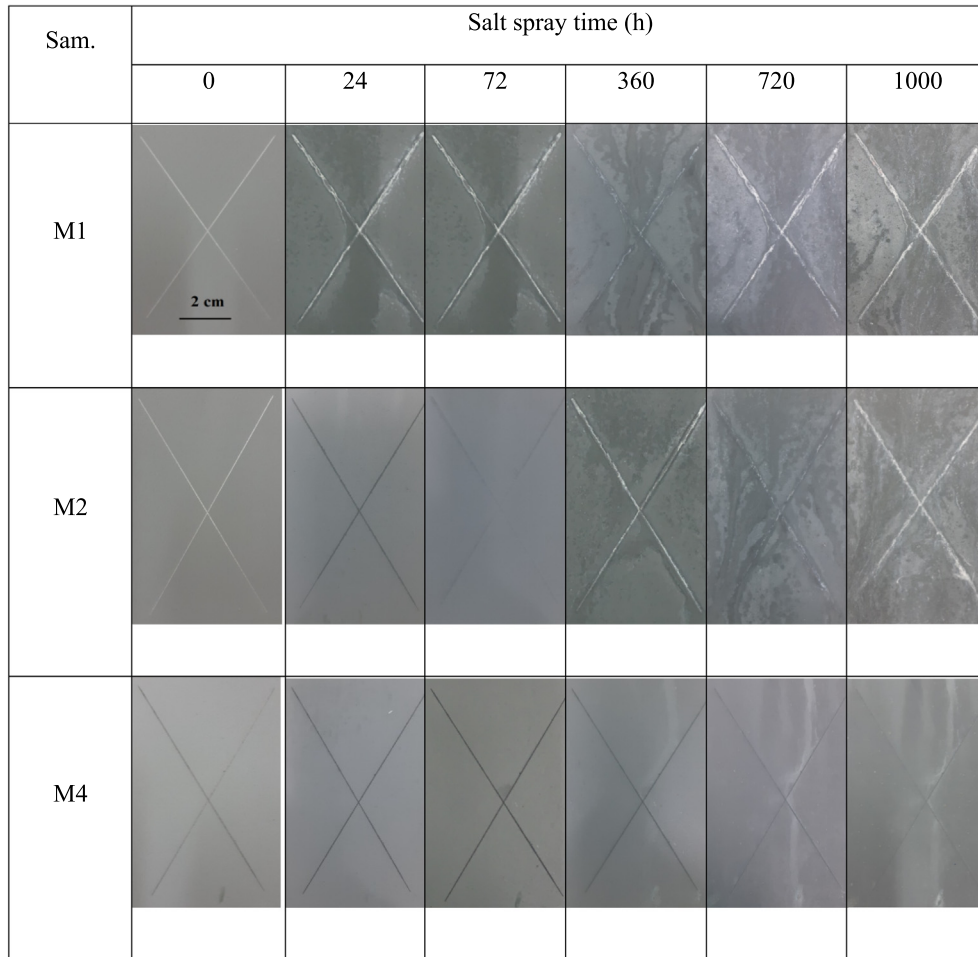

Fig. 7 Surface images of the silicate coating after the salt spray test for 1000 h.

tion of electrolyte penetration to the coating/substrate interface. The bonding matrix between the zinc and silicate creates an electrical contact between the zinc particles and the zirconium conversion layer that reduces the electrochemical reac-

tions at the anodes and cathodes on the substrate metal surface (Askari et al., 2014; Saeedikhani et al., 2019), leading to a decrease in the formation of corrosion products below the coating.
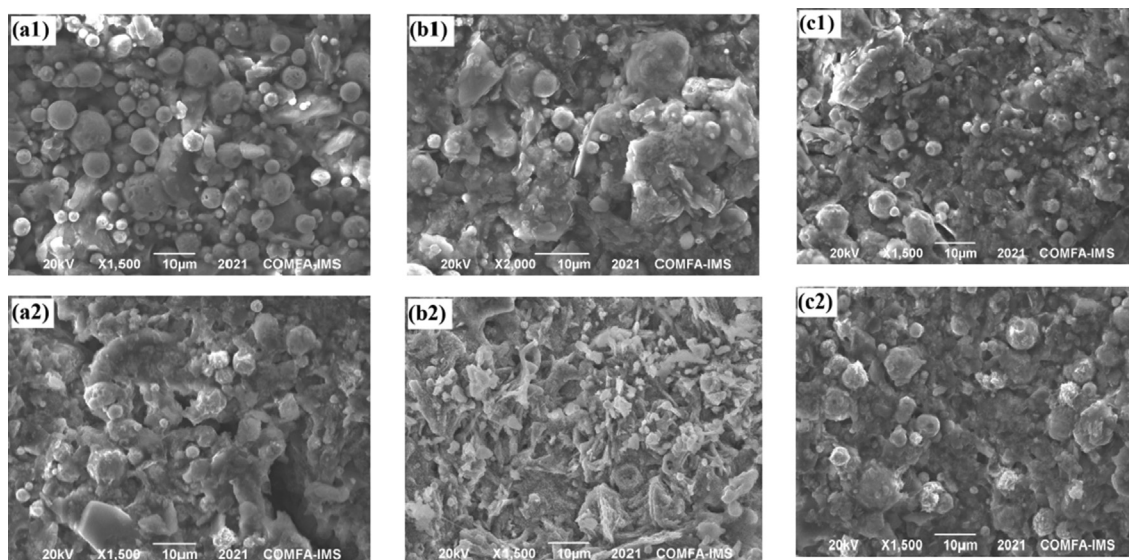
Fig. 8   SEM images of samples M1 (a1 and a2), M2 (b1 and b2) and M4 (c1 and c2) before (upper) and after (under) salt spray test for 1000 h.

3.3.4. Pull-off adhesion tests

The adhesive strength of the silicate coatings before and after the salt spray test is shown in Fig. 9. The results show that the decrease in the adhesive strength of sample M2 is less than that of sample M1, confirming that the flake ZnAl pigment is effective in improving inhibition of electrolyte penetration to the substrate surface, leading to an increase in the adhesive strength of the coating. Sample M4 with the zirconium pretreatment has the lowest adhesion loss, confirming that the protection of the zirconium conversion coating enhances the anodic and cathodic sites and improves the adhesion and delamination resistance compared to the non-pretreated samples (Alibakhshi et al., 2017).

4. Conclusions

This study demonstrated the effective use of flake ZnAl alloy pigment and zirconium pretreatment in improving the corrosion protection properties of silicate coatings. The properties of the zirconium conversion coating and the replacement of spherical zinc particles by flake
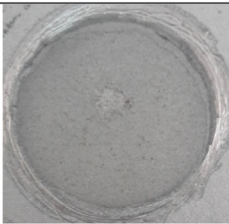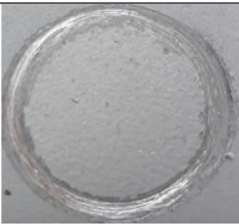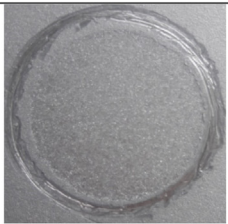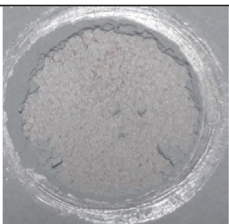
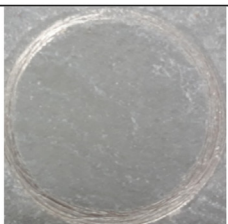| Samples	M1	M2	M4
Before salt spray test	3.32 ± 0.15 (MPa)	3.71 ± 0.15 (MPa)	3.96 ± 0.16 (MPa)
After salt spray test	2.24 ± 0.10 (MPa)	3.10 ± 0.23 (MPa)	3.46 ± 0.25 (MPa)
Adhesion loss (%)	32.53	16.53	12.54

Fig. 9   Surface images and adhesion strength of the pull-off adhesion test for different samples before and after the salt spray test (1000 h).

ZnAl alloy were investigated. Zinc-rich silicate coatings containing the flake ZnAl pigment improve the corrosion protection properties. The salt spray test and surface morphology show that the flake ZnAl pigment prolongs cathodic protection. In addition, the silicate coating containing flake ZnAl pigment pretreated with a zirconium conversion layer significantly reduces the formation of corrosion products and increases the adhesive strength of the coating. Therefore, the combination of the barrier properties of the flake ZnAl pigments and the reduction in anodic and cathodic active sites in the zirconium conversion layer enhances corrosion resistance and extends the duration of protection of the metal.

Funding

Declaration of Competing Interest

The authors declare that they have no known competing financial interests or personal relationships that could have appeared to influence the work reported in this paper.

Appendix A. Supplementary data

Supplementary data to this article can be found online at https://doi.org/10.1016/j.arabjc.2022.103815.

References

Abdelsalam, M.M., Bedair, M.A., Hassan, A.M., et al, 2022. Green synthesis, electrochemical, and DFT studies on the corrosion inhibition of steel by some novel triazole Schiff base derivatives in hydrochloric acid solution. Arabian J. Chem. 15, 103491.

Abreu, C., Izquierdo, M., Keddam, M., et al, 1996. Electrochemical behaviour of zinc-rich epoxy paints in 3% NaCl solution. Electrochim. Acta 41, 2405–2415.

Ahadi, M.M., Attar, M.M., 2007. OCP measurement: a method to determine CPVC. Scientia Iranica. 14, 369–372.

Alibakhshi, E., Ghasemi, E., Mahdavian, M., et al, 2017. A comparative study on corrosion inhibitive effect of nitrate and phosphate intercalated Zn-Al-layered double hydroxides (LDHs) nanocontainers incorporated into a hybrid silane layer and their effect on cathodic delamination of epoxy topcoat. Corros. Sci. 115, 159–174.

Arman, S., Ramezanzadeh, B., Farghadani, S., et al, 2013. Application of the electrochemical noise to investigate the corrosion resistance of an epoxy zinc-rich coating loaded with lamellar aluminum and micaceous iron oxide particles. Corros. Sci. 77, 118–127.

Asemani, H., Ahmadi, P., Sarabi, A., et al, 2016. Effect of zirconium conversion coating: Adhesion and anti-corrosion properties of epoxy organic coating containing zinc aluminum polyphosphate (ZAPP) pigment on carbon mild steel. Prog. Org. Coat. 94, 18–27.

Askari, F., Ghasemi, E., Ramezanzadeh, B., et al, 2014. Mechanistic approach for evaluation of the corrosion inhibition of potassium zinc phosphate pigment on the steel surface: application of surface analysis and electrochemical techniques. Dyes Pigm. 109, 189–199.

Bajat, J., Mišković-Stanković, V., Popić, J.P., et al, 2008. Adhesion characteristics and corrosion stability of epoxy coatings electrodeposited on phosphated hot-dip galvanized steel. Prog. Org. Coat. 63, 201–208.

Barranco, V., Feliu Jr, S., Feliu, S., 2004. EIS study of the corrosion behaviour of zinc-based coatings on steel in quiescent 3% NaCl solution. Part 1: directly exposed coatings. Corros. Sci. 46, 2203–2220.

Canosa, G., Alfieri, P.V., Giudice, C.A., 2012. Environmentally friendly, nano lithium silicate anticorrosive coatings. Prog. Org. Coat. 73, 178–185.

Cheng, L., Liu, C., Han, D., et al, 2019. Effect of graphene on corrosion resistance of waterborne inorganic zinc-rich coatings. J. Alloy. Compd. 774, 255–264.

Del Amo, B., Romagnoli, R., Deyá, C., et al, 2002. High performance water-based paints with non-toxic anticorrosive pigments. Prog. Org. Coat. 45, 389–397.

Deya, C., Blustein, G., Del Amo, B., et al, 2010. Evaluation of eco-friendly anticorrosive pigments for paints in service conditions. Prog. Org. Coat. 69, 1–6.

Fedrizzi, L., Rodriguez, F., Rossi, S., et al, 2001. The use of electrochemical techniques to study the corrosion behaviour of organic coatings on steel pretreated with sol–gel zirconia films. Electrochim. Acta 46, 3715–3724.

Feliu Jr, S., Barranco, V., 2003. XPS study of the surface chemistry of conventional hot-dip galvanised pure Zn, galvanneal and Zn–Al alloy coatings on steel. Acta Mater. 51, 5413–5424.

Feliu, S., Morcillo, M., 2001. Deterioration of cathodic protection action of zinc-rich paint coatings in atmospheric exposure. Corrosion. 57, 591–597.

Fockaert, L., Taheri, P., Abrahami, S., et al, 2017. Zirconium-based conversion film formation on zinc, aluminium and magnesium oxides and their interactions with functionalized molecules. Appl. Surf. Sci. 423, 817–828.

Giudice, C., Benitez, J., Pereyra, A., 2004. Influence of extender type of performance of modified lamellar zinc primers. JCT Res. 1, 291–304.

Golabadi, M., Aliofkhazraei, M., Toorani, M., 2021. Corrosion behavior of zirconium-pretreated/epoxy-coated mild steel: New approach for determination of cathodic disbondment resistance by electrochemical impedance spectroscopy. J. Alloy. Compd. 873, 159800.

Golru, S.S., Attar, M., Ramezanzadeh, B., 2015. Morphological analysis and corrosion performance of zirconium based conversion coating on the aluminum alloy 1050. J. Ind. Eng. Chem. 24, 233–244.

Grundmeier, G., Schmidt, W., Stratmann, M., 2000. Corrosion protection by organic coatings: electrochemical mechanism and novel methods of investigation. Electrochim. Acta 45, 2515–2533.

Hosseini, R.M., Sarabi, A., Mohammadloo, H.E., et al, 2014. The performance improvement of Zr conversion coating through Mn incorporation: With and without organic coating. Surf. Coat. Technol. 258, 437–446.

Ishimura, T., Lu, R., Yamasaki, K., et al, 2010. Development of an eco-friendly hybrid lacquer based on kurome lacquer sap. Prog. Org. Coat. 69, 12–15.

Jalili, M., Rostami, M., Ramezanzadeh, B., 2015. An investigation of the electrochemical action of the epoxy zinc-rich coatings containing surface modified aluminum nanoparticle. Appl. Surf. Sci. 328, 95–108.

Kakaei, M., Danaee, I., Zaarei, D., 2013a. Investigation of corrosion protection afforded by inorganic anticorrosive coatings comprising micaceous iron oxide and zinc dust. Corros. Eng., Sci. Technol. 48, 194–198.

Kakaei, M.N., Danaee, I., Zaarei, D., 2013b. Evaluation of cathodic protection behavior of waterborne inorganic zinc-rich silicates containing various contents of MIO pigments. Anti-Corros. Methods Mater. 60, 37–44.

Kalendova, A., 2002. Mechanism of the action of zinc-powder in anticorrosive coatings. Anti-Corros. Methods Mater. 49, 173–180.

Kalendová, A., 2003. Effects of particle sizes and shapes of zinc metal on the properties of anticorrosive coatings. Prog. Org. Coat. 46, 324–332.

Marchebois, H., Savall, C., Bernard, J., et al, 2004. Electrochemical behavior of zinc-rich powder coatings in artificial sea water. Electrochim. Acta 49, 2945–2954.

Meroufel, A., Touzain, S., 2007. EIS characterisation of new zinc-rich powder coatings. Prog. Org. Coat. 59, 197–205.

Mohammadloo, H.E., Sarabi, A.A., Alvani, A.A.S., et al, 2012. Nano-ceramic hexafluorozirconic acid based conversion thin film: Surface characterization and electrochemical study. Surf. Coat. Technol. 206, 4132–4139.

Montemor, M., Simões, A., Ferreira, M., et al, 2000. The corrosion performance of organosilane based pre-treatments for coatings on galvanised steel. Prog. Org. Coat. 38, 17–26.

Parashar, G., Bajpayee, M., Kamani, P., 2003. Water-borne non-toxic high-performance inorganic silicate coatings. Surf. Coat. Int. Part B: Coat. Trans. 86, 209–216.

Rajan, R., Zakaria, Y., Shamsuddin, S., et al, 2020. Robust synthesis of mono-dispersed spherical silica nanoparticle from rice husk for high definition latent fingermark development. Arabian J. Chem. 13, 8119–8132.

Ramanathan, E., Balasubramanian, S., 2016. Comparative study on polyester epoxy powder coat and amide cured epoxy liquid paint over nano-zirconia treated mild steel. Prog. Org. Coat. 93, 68–76.

Saarimaa, V., Kaleva, A., Ismailov, A., et al, 2021. Corrosion product formation on zinc-coated steel in wet supercritical carbon dioxide. Arabian J. Chem. 103636.

Sababi, M., Terryn, H., Mol, J., 2017. The influence of a Zr-based conversion treatment on interfacial bonding strength and stability of epoxy coated carbon steel. Prog. Org. Coat. 105, 29–36.

Saeedikhani, M., Wijesinghe, S.L., Blackwood, D.J., 2019. Barrier and Sacrificial Protection Mechanisms of Zinc Rich Primers. Eng. J. 23, 223–233.

Selvaraj, M., Guruviah, S., 1997. The electrochemical aspects of the influence of different binders on tne corrosion protection afforded by zinc-rich paints. Surf. Coat. Int. 80, 12–17.

Shreepathi, S., Bajaj, P., Mallik, B., 2010. Electrochemical impedance spectroscopy investigations of epoxy zinc rich coatings: Role of Zn content on corrosion protection mechanism. Electrochim. Acta 55, 5129–5134.

Szociński, M., Darowicki, K., 2016. Performance of zinc-rich coatings evaluated using AFM-based electrical properties imaging. Prog. Org. Coat. 96, 58–64.

Trabelsi, W., Cecílio, P., Ferreira, M., et al, 2007. Surface evaluation and electrochemical behaviour of doped silane pre-treatments on galvanised steel substrates. Prog. Org. Coat. 59, 214–223.

Trabelsi, W., Dhouibi, L., Triki, E., et al, 2005. An electrochemical and analytical assessment on the early corrosion behaviour of galvanised steel pretreated with aminosilanes. Surf. Coat. Technol. 192, 284–290.

Van Ooij, W., Zhu, D., Stacy, M., et al, 2005. Corrosion protection properties of organofunctional silanes—an overview. Tsinghua Sci. Technol. 10, 639–664.

Verdier, S., Delalande, S., Van Der Laak, N., et al, 2005. Monochromatized x-ray photoelectron spectroscopy of the AM60 magnesium alloy surface after treatments in fluoride-based Ti and Zr solutions. Surface and Interface Analysis: An International Journal devoted to the development and application of techniques for the analysis of surfaces, interfaces and thin films 37, 509–516.

Xanthos, M., 2010. Functional fillers for plastics. John Wiley & Sons.

Xia, W., Chen, Z., Zhang, G., et al, 2021. Comparison of cathodic protection processes of 40% zinc-rich coatings under immersion and atmospheric conditions: Protection for defective areas. Electrochim. Acta 385, 138450.

Xu, R., He, T., 2019. Corrosion of self-curing waterborne zinc oxide-potassium silicate coating modified with aluminium powder. J. Alloy. Compd. 811, 152008.

Zand, B.N., Mahdavian, M., 2007. Evaluation of the effect of vinyltrimethoxysilane on corrosion resistance and adhesion strength of epoxy coated AA1050. Electrochim. Acta 52, 6438–6442.

Zhai, Y., Z. Zhao, G. Frankel, et al., 2007. Surface pretreatment based on dilute hexafluorozirconic acid. Department of Defense. Proceedings of the Corrosion Conference.

Zhan, W., Liu, X., Lu, C., et al, 2017. The Property of Colored Chemical Conversion on Various Metals with Iso-solution. Procedia Eng. 174, 341–346.

Zhang, L., Ma, A., Jiang, J., et al, 2012. Anti-corrosion performance of waterborne Zn-rich coating with modified silicon-based vehicle and lamellar Zn (Al) pigments. Progr. Natural Sci.: Mater. Int. 22, 326–333.

Zhang, W., Wang, J., Li, Y.-N., et al, 2010. Evaluation of metal corrosion under defective coatings by WBE and EIS technique. Acta Phys. Chim. Sin. 26, 2941–2950.